THE JOURNAL OF COMPARATIVE NEUROLOGY 387:325–340 (1997)

Natural Variability in the Number of Dendritic Segments: Model-Based Inferences About Branching During Neurite Outgrowth

JAAP VAN PELT,[1]* ALEXANDER E. DITYATEV,[2] AND HARRY B.M. UYLINGS[1]
[1]Graduate School Neurosciences Amsterdam, Netherlands Institute for Brain Research, 1105 AZ Amsterdam, The Netherlands
[2]Department of Molecular Neurobiology, University of Hamburg, 20251 Hamburg, Germany

ABSTRACT

A study was made of the possible basis for naturally occurring variations in the number of segments in individual dendritic trees. Distributions of the number of terminal segments have been studied in dendrites from rat, cat, and frog motoneurons, basal dendrites from rat visual cortex pyramidal and non-pyramidal neurons, in rat cerebellar Purkinje cell dendritic trees, and in human hippocampal dentate granule cells. By means of a mathematical model for dendritic branching, it was shown that the variation in the number of dendritic segments can be accounted for by assuming that new branches during neurite outgrowth are formed randomly at terminal segments. The observed terminal segment number distributions could be closely approximated by additionally assuming that branching probabilities decline with increasing number of terminal segments in growing dendrites. The pyramidal neuron group differed significantly from the other neuron groups in such a way as to suggest that this decline is stronger than in the dendrites of other types of neurons. By using literature data on the mean number of terminal segments in rat cerebellar Purkinje cells, measured at different times during early development, an estimate could be obtained of the time-course of the branching probabilities. The branching probability of a terminal segment was found to be in the order of 0.002 per hour in the first 4 weeks postnatal with a 5-fold transient increase in the second week. J. Comp. Neurol. 387:325–340, 1997.

Indexing terms: pyramidal neuron; Purkinje neuron; motoneurons; dentate granule cells; growth model

Dendritic branching patterns are complex and show a large degree of variation in their shapes, within, as well as between, different cell types and species. This variation can be found in typical shape parameters, such as the number, length, and connectivity pattern (topological structure) of the segments comprising the dendritic tree. The developmental processes underlying these large variations are poorly understood, e.g., to what extent they are the direct result of specific genetic programs or result merely from random processes. From this consideration, the question arises as to the minimal requirements for specification of growth parameters so as to closely approximate observed morphological characteristics and variations.

Characteristic dendritic branching patterns emerge during neuronal development from the behavior of growth cones, the structures that determine the process of branching and lengthening of the constituent segments of the tree (e.g., Bray, 1992). This dynamic behavior of growth cones is the result of cellular responses to the local environment (e.g., Kater et al., 1994; Letourneau et al., 1994). Local environments differ such that each growth cone has to respond individually (and perhaps independently) on the basis of local cues. In view of the large number of mechanisms involved in growth cone behavior, it is plausible to hypothesize that dendritic arborizations emerge from independent and stochastic behavior of growth cones.

One characteristic source of variation is the topological structure of dendrites. A branching pattern has a topological structure, or tree type, that is one out of a finite number

Grant sponsor: NATO; Grant number: CRG 930426.

*Correspondence to: Dr. Jaap van Pelt, Netherlands Institute for Brain Research, Meibergdreef 33, 1105 AZ Amsterdam.
E-mail: j.van.pelt@nih.knaw.nl

Received 20 March 1996; Revised 29 April 1997; Accepted 9 May 1997

of theoretical possibilities. Topological differences among dendritic branching patterns are, therefore, represented by the frequencies of occurrence of all such possible tree types. Random branching, based on random selection of the branching segment among the existing ones in the tree, indeed results in large and characteristic variations in the topological structures of dendritic trees. This has initially been demonstrated for two specific modes of random branching, i.e., occurring 1) exclusively at terminal segments or 2) at all segments in a tree (e.g., Berry and Bradley, 1976; Van Pelt and Verwer, 1983). The general finding was that the first mode of branching (random terminal growth) was in better agreement with the observed incidence of different tree types than the second one (random segmental growth). Van Pelt and Verwer (1986) subsequently developed a generalized growth model in which the probability of a segment to be selected for branching was made dependent on 1) the type of the segment (intermediate or terminal), and 2) the position of the segment (centrifugal order) within the tree. With this model, they could accurately account for the observed topological variations found in dendrites from rat cerebellar Purkinje cells, rat cortical pyramidal, and multipolar non-pyramidal cells (Van Pelt et al., 1992). This agreement could be obtained by incorporating either a slight contribution by intermediate segments to the branching process or a moderate dependence of the branching probability on the topological distance of the segment from the cell body. Similar results were obtained by Dityatev et al. (1995), who analysed topological variations in motoneuronal dendrites from rat, cat, and frog, by using the same growth model approach. These findings have provided strong support for the hypothesis that dendritic development proceeds stochastically by means of independently behaving growth cones. These findings also imply that the minimal assumptions for accounting for observed topological variations reduce to the underlying probabilities for segments to branch.

Although topological variance in dendrites thus appears to be highly dependent on the mode of initial outgrowth, it nevertheless is a robust property with respect to subsequent pruning. Van Pelt (1997) showed that removal of uniform randomly selected segments or subtrees resulted in trees, the topological variation of which was still fully consistent with the mode of growth that was postulated for the original complete trees. Under the given condition, this should also apply for the retraction of branches during development or loss of branches during sectioning.

Dendrites show also a large variation in the number of terminal segments (or, equivalently, in the number of bifurcation points). For instance, the measured number of terminal segments per dendritic tree ranges between 1 and about 13 for rat visual cortex pyramidal neurons (Larkman, 1991), between 2 and about 49 for cat hindlimb motoneurons (Ulfhake et al., 1988), and between approximately 375 and 525 for 1-month-old rat cerebellar Purkinje cells (Woldenberg et al., 1993). This variation, clearly dependent on the cell type, is a direct result of a varying number of branching events experienced by the tree during its development. The hypothesis that dendritic arborizations can be fully accounted for by stochastically behaving growth cones should also apply for the variable occurrence of branching events in time. More specifically, the question has to be answered whether the observed variation in number of terminal segments per dendritic tree can be accounted for by assuming that the growth cones branch at random points in time. This question will be addressed for sets of dendritic trees obtained from a variety of cell types and species, the data for which were either taken from the literature or made available by other investigators (see next section). The random branching hypothesis will be tested by extending the present growth model, describing the selection process of the branching segment among all existing ones so as to also include a stochastic rule describing when a branching event will occur during development. It will be shown that the observed variations in the number of terminal segments per dendritic tree can be accounted for accurately by assuming branching events to occur randomly in time. In the following section, the empirical data used for the analysis will be presented, followed by a brief review of the topological growth model. Finally, the new extensions will be introduced in a step-wise manner.

MATERIALS AND METHODS

Empirical distributions of the number of terminal segments in dendritic trees

The terminal segment number data, used in this study, are obtained from different sources. The motoneuron data are obtained from a compilation by Dityatev et al. (1995), used in a study of the topology and growth rules of motoneuronal dendrites. They are derived from published data or from raw data used in the publications cited below, which were kindly provided by some of these authors. The dendrites of gastrocnemius and soleus motoneurons of adult cats (Cullheim et al., 1987), including unpublished data from S. Cullheim, J.W. Fleshman, L.L. Glenn, and R.E. Burke; the dendrites of lumbar motoneurons of young rats (9–13 days; Chmykhova et al., 1987), including unpublished data from O.A. Karamyan; dendrites of triceps surae motoneurons of adult rats (Chen and Wolpaw, 1994), including unpublished data from X.Y. Chen; the dendrites of motoneurons in organotypic cultures of rat spinal cord (Ulrich et al., 1994), including unpublished data from D. Ulrich; lumbar motoneuron dendrites of frogs *Rana ridibunda* (Babalian and Chmykhova, 1987), including unpublished data from N.M. Chmykhova; and motoneurons of frogs *Rana esculenta* (Birinyi et al., 1992), including unpublished data from M. Antal were used, as well as cultured neonatal rat striatum cholinergic interneurons (Studer et al., 1994), including unpublished data from L. Studer.

Terminal segment number distributions of completely reconstructed, intracellularly stained basal dendrites in rat cortical layer 2/3, thick layer 5, and slender layer 5 pyramidal neurons were obtained from Figure 3 in Larkman (1991). Golgi-Cox data of visual cortex Layer 2/3 pyramidal cell basal dendrites from 30 days and 150-day-old rats, and of visual cortex multipolar nonpyramidal dendrites from 150-day-old rats were kindly provided by H.B.M. Uylings (see Uylings et al., 1990).

Dendrites of control groups of aged and adult human fascia dentata granule cells were obtained from De Ruiter and Uylings (1987), and from unpublished data of a study of L. Mrzljak and Uylings at the NIBR, Amsterdam (also see Seress and Mrzljak, 1987).

Terminal segment number data from rat Purkinje cell dendritic trees were obtained from Figure 4 of Woldenberg et al. (1993), encompassing the distributions of four age

groups, viz. 1, 10, 18, and 28 months postnatally. The means and standard deviations for the number of terminal segments per dendrite are derived from the lumped terminal segment number distributions in this figure.

The shapes of the terminal segment number distributions of all the above-mentioned dendrite data sets are displayed in Figure 5 as continuous histogram lines. The means and standard deviations of these terminal segment number distributions, in the following indicated by *mean* and *sd*, are given in Table 1, column 3 and 4. Additionally, the *means* and *sds* for rat Purkinje cell dendritic trees of five age groups (5, 10, 15, 30, and 50 days; see Berry and Bradley, 1976) are included in Table 1.

Topological trees

For the topological characterization, dendrites are reduced to their skeleton of segments, maintaining their particular pattern of connectivity (i.e., tree type). Metrical properties are ignored. A topological tree is thus characterized by its number of segments and its tree type. Terminal and intermediate segments are distinguished according to whether they end in a terminal tip or in a bifurcation point, respectively. The proximal/distal postition of a segment in the tree is denoted by its centrifugal order, indicating the number of bifurcation points on the path from the soma up to the pertinent segment. Thus, the root segment has centrifugal order zero and, when it ends in a bifurcation point, its daughter segments will have centrifugal order one, etc. The number of terminal segments in a tree will, in the following, be denoted as the degree of the tree.

An efficient measure for the topological structure appears to be the tree-asymmetry index (Van Pelt et al., 1992). For a tree of degree n, the index is defined by

$$A_t(\alpha^n) = \frac{1}{n-1}\sum_{j=1}^{n-1} A_p(r_j, s_j), \qquad (1)$$

being the mean value of the partition asymmetries in the tree, which, at each of the $n-1$ bifurcation points, indicate the relative difference in the number of terminal segments r_j and s_j in the two subtrees emerging from the jth bifurcation point. The partition asymmetry A_p at a bifurcation is defined as

$$A_p(r, s) = \frac{|r-s|}{r+s-2} \qquad (2)$$

for $r + s > 2$ and with $A_p(1, 1) = 0$, by definition. The tree asymmetry index equals zero when at each bifurcation the two subtrees in the pair have an equal number of terminal segments (maximal symmetry) and approaches one for large trees, when in each subtree pair one of the two subtrees is just one terminal segment (maximal asymmetry).

Modeling the growth of dendritic branching patterns

In the following sections, the construction of the growth model is introduced in a stepwise manner, so as to clearly show the results of the assumptions made in the growth rules with respect to the eventual variation in the number of terminal segments per dendrite. The original, so-called QS-model will first be discussed and its ability to correctly predict the variation in topological tree types after a given number of branching events. Next, dendritic growth will be introduced as a random branching process on a series of time periods (denoted as time-bins) to arrive at a correct description of the variation in the number of terminal segments per dendrite. Finally, the growth process will be defined on a real time scale in order to obtain a correct description of the time course of the mean of the terminal segment number distribution.

Modeling dendritic growth as a sequence of branching events at randomly selected segments (QS-model)

The QS-model, developed by Van Pelt and Verwer (1986), describes dendritic growth as a series of branching events. At each branching event a new (terminal) segment is attached to one of the existing segments. The selection of the segment for branching is assumed to be determined by a random process, based on a scheme of branching probabilities. These probabilities may differ between intermediate and terminal segments and may depend on the topological distance of the segment from the cell body (centrifugal order). The branching probability p_{term} of a terminal segment at centrifugal order γ is defined by $p_{term} = C_1 2^{-S\gamma}$, with parameter S modulating the dependence on centrifugal order, and C_1 being a normalization constant to make the sum of the branching probabilities of all the segments in the tree equal to one. For $S = 0$, all terminal segments have the same probability for being selected for branching. For $S = 1$, the branching probability of a terminal segment will decrease by a factor of two for each following order. The branching probability of an intermediate segment p_{int} relates to that of a terminal segment of the same order via $p_{int} = \frac{Q}{1-Q} p_{term}$, with Q a parameter having values between 0 and 1. The parameter Q roughly indicates the total branching probability for all intermediate segments in a tree, with $Q = 0$ (no branching of intermediate segments) and $Q = 1$ (branching of intermediate segments only).

After $n - 1$ branching events, a tree will be formed having $n - 1$ bifurcation points, $n - 1$ intermediate and n terminal segments, and with a connectivity pattern (tree type), which is one out of a finite number of possible tree types with n terminal segments. The randomness in the selection of the segment for branching makes the actual sequence of branching events, and thus the final tree type, also the result of a random process. An example of two such sequences of seven branching events is given in Figure 1 for the random terminal growth mode, in which only terminal segments can branch (all of them with equal probability) (Q, S) = (0,0). The frequencies of occurrence of the various tree types depend upon the mode of growth, as determined by the parameter values Q and S, and also result in a characteristic value for the mean tree-asymmetry index. For the random terminal growth mode, the expected value for the tree-asymmetry index is equal to 0.46. Lower tree-asymmetry values are expected when terminal segments, proximal to the soma, have a higher branching probability than distal terminal segments. Higher tree-asymmetry values in turn occur, either when predominantly distal terminal segments branch, or when intermediate as well as terminal segments branch.

For optimal parameter values, the QS-model accurately reproduces the topological variation observed in natural dendrites (i.e., the frequency distribution of different tree

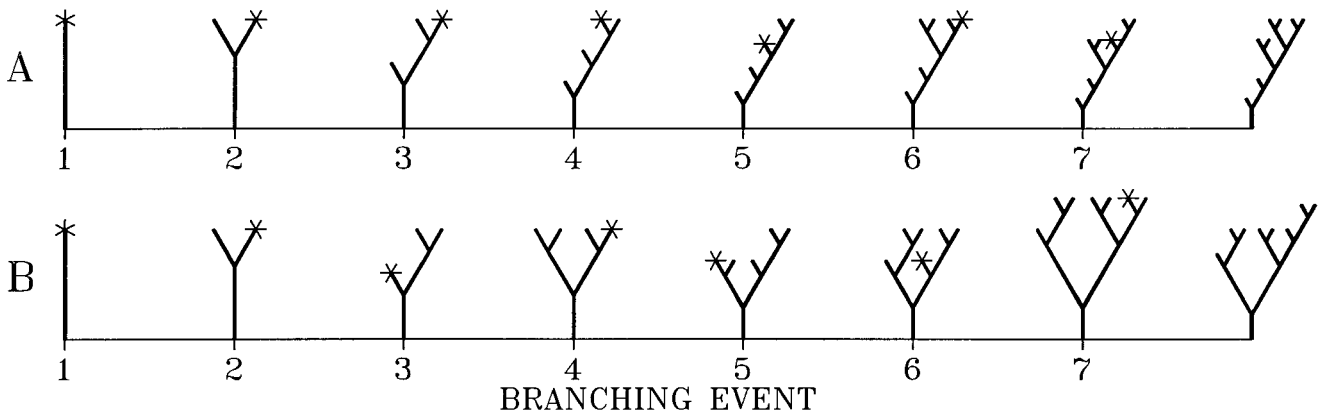

Fig. 1. Growth of a branching pattern depicted as a sequence of branching events. At each branching event, one of the terminal segments is randomly selected for branching (indicated by asterisk) according to a uniform probability distribution (random terminal growth mode). After seven branching events, trees are formed with eight terminal segments. The randomness in branching has resulted in two different sequences A and B, ending in different topological tree types. The trees are depicted in a standardized way, such that, at each bifurcation point, the left subtree has a rank number, lower than or equal to the rank number of the right subtree (Van Pelt and Verwer, 1983).

types with a given number of terminal segments; Van Pelt and Verwer, 1986; Van Pelt et al., 1992; Dityatev et al., 1995). For both the pyramidal and the motoneuron cell groups values were found for the tree-asymmetry index close to or slightly lower than 0.46, thus suggesting a process of random terminal branching with a possibly slight dominance of proximal terminal segments. Thus, these authors have demonstrated that the assumption of random sequential branching is sufficient to explain the observed topological variability in dendritic trees with equal number of terminal segments. Additionally, Dityatev et al. (1995) showed that, like the tree-asymmetry index, other properties, which depend upon the topological structures, such as the maximal and the mean centrifugal order of the segments, the partition frequencies (i.e., the number of terminal segments in subtree pairs at bifurcation points), and the relationship between mean centrifugal order and number of terminal segments for a given set of trees, were correctly reproduced by the QS-model.

Dityatev et al. (1995) rightly pointed out the incompleteness of the QS-model in the sense that it does not consider the variation in the number of terminal segments per dendritic tree. Indeed, the QS-model was designed to explain the topological variation in trees after a given number of branching events, but not the variation in the number of branching events during a given period of time. In the next sections, the QS-model will be extended by formulating growth as a stochastic process in time. The number of branching events after a given time period then becomes also a variable quantity. Based on the results of the topological studies (Van Pelt et al., 1992; Dityatev et al., 1995), we will assume in the following that branching occurs at terminal segments only.

Modeling dendritic growth as a random branching process in time

As argued above, branching will be assumed to occur exclusively at terminal segments (i.e., $Q = 0$). We will consider a growth process over a developmental period T. This period is divided into N short periods, called time-bins with, not necessarily equal, durations T_i, which add up to the total duration $T (\sum_{i=1}^{N} T_i = T)$. For each time-bin i, branching probabilities p_i for the terminal segments will be defined. The number N will be chosen large enough that the branching probability per terminal segment per time-bin is much smaller than unity. Then, it is unlikely that a given segment will branch more than once per time-bin. The branching probability per unit of time follows from p_i/T_i. The first steps concern the definition of the branching probabilities per time-bin. It will be shown that these steps result in a realistic description of the shape of the degree distribution, and thus of the variation in terminal segment number. The last steps concern the definition of the time-bin durations, which allow for a realistic description of the time course of the degree distribution during development, maintaining the correct shapes at the different points in time.

Step 1. Constant branching probability (B-model). First, it will be assumed that the branching probability *p* of terminal segments per time-bin remains constant during the growth process. The expected number of branching events B of a single terminal segment during the whole developmental period T is then equal to $B = pN$. In the following, we will take B as a parameter of the model and we obtain p via

$$p = B/N. \tag{3}$$

The growth rate per time-bin, the mean (i.e., expected) number of branching events $\overline{\Delta n_i}$ in a tree with n_i terminal segments at time-bin i equals

$$\overline{\Delta n_i} = n_i p = n_i B/N. \tag{4}$$

The number of actually occurring branching events per time-bin increases the number of terminal segments accordingly, so that an increasing number of terminal segments comes to participate in the branching process. Two examples of growth sequences are depicted in Figure 2 for the parameter values $B = 3$ and $N = 200$. The branching probability per terminal segment per time-bin then equals $p = B/N = 3/200$, being much smaller than unity. The stochastic nature of the branching process is reflected in

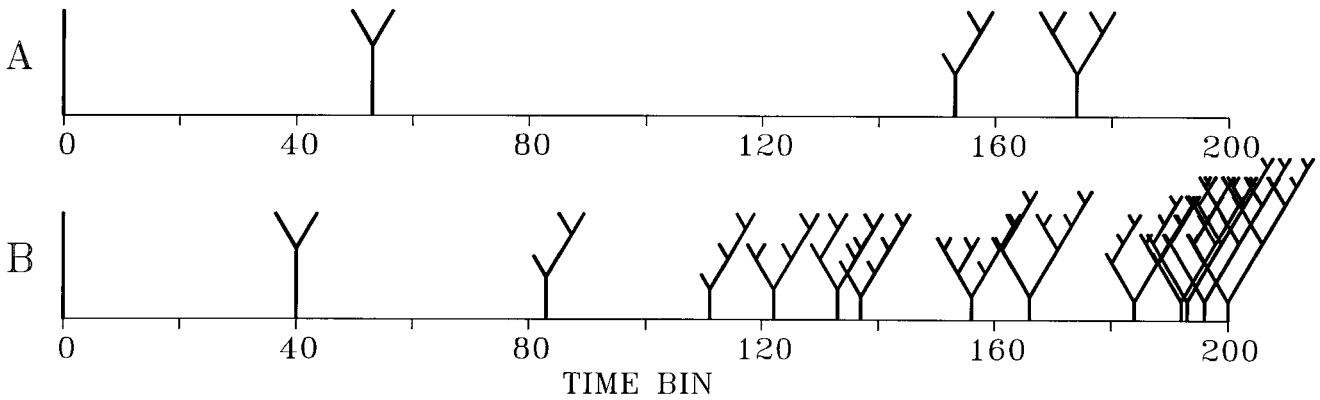

Fig. 2. Growth of a branching pattern versus a time-bin scale. The full time period is divided into N = 200 time-bins. At each time-bin, any of the terminal segments in the growing tree may branch with a constant probability *p*. When a branching event has actually occurred, the new tree is plotted at the time-bin of concern. The branching probability p is defined by p = B/N with B the expected number of branching events of a single terminal segment during the full period. The two examples, calculated for B = 3, N = 200, and thus for p = 0.015, demonstrate how individual growth courses may differ because of the randomness in branching and how the final trees may differ in the number of terminal segments. Additionally, they show that the number of branch points in the final trees can be (much) larger than the value of B = 3, because of the proliferation in the number of terminal segments during growth.

the variation in the two different growth sequences, and in the large difference in degree in the final trees.

Figure 2A shows a sequence with only a few branching events. Figure 2B shows a sequence with a rapid proliferation of the number of terminal segments and a clearly increasing growth rate. Thus, at the end of the period T the same growth rule results in trees of highly different size. A broad distribution for the number of terminal segments per tree is therefore expected when many trees are produced by this growth model. This is indeed shown in Figure 3A with degree distributions for parameter values B = 1, 2, 3, and 4. All the distributions are monotonously decreasing with increasing degree and have long tails for even small values of the parameter B. These shape characteristics are, however, quite different from those of the observed degree distributions, which are unimodal and do not have large tails (see Fig. 5). Thus, although the assumption of constant branching probabilities per terminal segment per time-bin (B-model) results in a substantial variation in the number of terminal segments in the final trees, the shape of the degree distribution is highly unrealistic.

Step 2. Degree-dependent branching probabilities (BE-model). The constant branching probability model produces large tails in the degree distribution because the rate of increase in the degree of the trees is proportional to the degree itself. To reduce such a growth accelerating effect we now assume that, in addition, the branching probability p_i of a terminal segment per time-bin i depends on the total number of terminal segments n_i in the tree,

$$p_i = B/Nn_i^E, \tag{5}$$

in which the exponent E modulates the strength of the degree dependency. For the growth rate, the expected number of branching events in the tree at time-bin i, $\overline{\Delta n_i}$, we obtain

$$\overline{\Delta n_i} = n_i p_i = Bn_i^{1-E}/N. \tag{6}$$

For E = 0, we again obtain the B-model, with $p_i = B/N$. For the value E = 1, in contrast, the branching probability per terminal segment per time-bin becomes $p_i = B/Nn_i$. Then, the expected number of branching events during time-bin i becomes $\overline{\Delta n_i} = B/N$, a constant, independent of the size of the tree, which shows that p is fully corrected for the effects of increasingly many terminal segments in the growing tree. The effect of degree-dependent branching probabilities is illustrated in Figure 3B showing that the long tails disappear for increasing values of E, while the unimodal distribution becomes increasingly narrower. The distributions in the figures have been calculated by means of a recurrent expression for the degree distribution which is given in the Appendix. The distributions in Figure 3A, B display a full range of shapes for different values of the parameters B and E. This is also illustrated in Figure 4 in which the (B, E) parameter grid is mapped onto the (mean, sd) plane. The map is obtained by calculating for many pairs of (B, E) parameter values the mean and standard deviation of the degree distribution, which are subsequently plotted as a point in the (mean, sd) plane. Points having equal E values are then connected so as to form continuous lines while points with equal B values are connected by dotted lines. Using the mean and sd of a set of observed trees, this map makes it easy to find those (B, E) parameter values that optimally reproduce the given mean and sd values. The family of E-curves (continuous lines) in the map shows how the variance is reduced by increasing values of E. The (B, E) parameter grid covers a large area of the (mean, sd)-plane, implying that any desired mean and sd within this area can be reproduced by an appropriate choice of (B, E) parameter values.

The BE-model is thus able to produce distributions for the number of terminal segments per dendrite with realistic values for both mean and sd. Whether the shape of the distributions is correctly reproduced as well will be discussed in the following sections.

Step 3. Degree- and order-dependent branching probabilities (BES-model). In the B-model and BE-model all terminal segments in a tree have equal probabilities for branching per time-bin. This mode of growth results in a variation in topological structures that is similar to that for the "random terminal growth mode" (Q, S) = (0, 0). The restriction of equal branching probabilities will now be

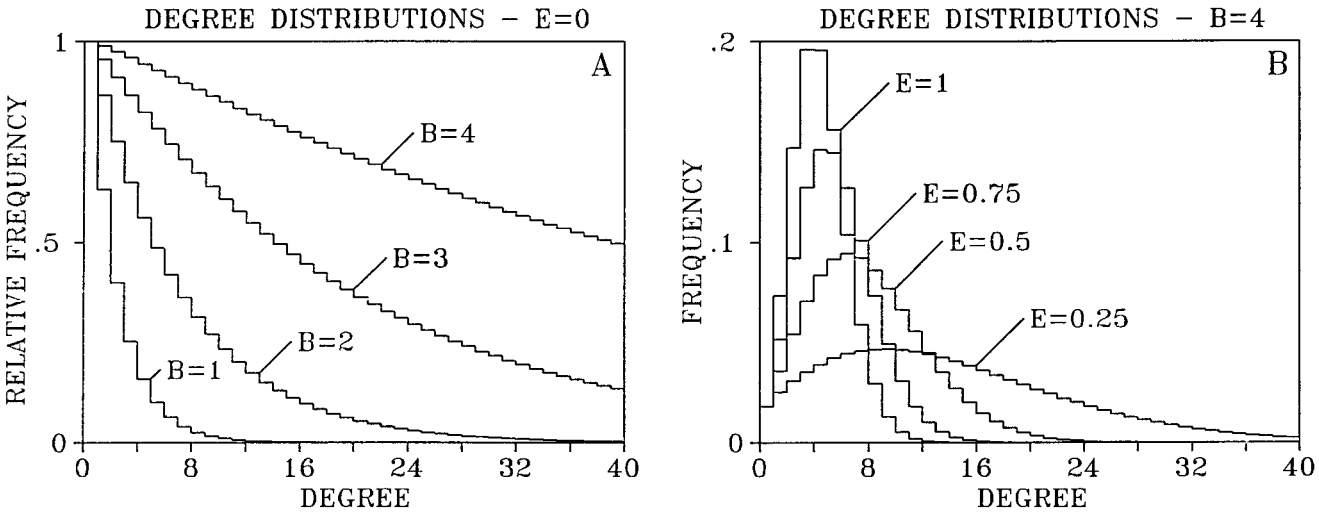

Fig. 3. **A:** Degree distributions of trees obtained by growth modes in which each terminal segment has a constant branching probability per time-bin p, given by p = B/N, with N = 500 and B = 1, 2, 3, or 4, respectively. **B:** Degree distributions of trees obtained by growth modes in which the branching probability p_i per terminal segment per time-bin i depends on the total number of terminal segments n_i with $p_i = B/Nn_i^E$, N = 500, B = 4, and E = 0.25, 0.5, 0.75, and 1.0, respectively. The distributions for E = 0 are monotonously decreasing, but become for E > 0 unimodal and narrower for increasing values of E.

relaxed by letting the branching probability of a terminal segment depend on both the degree of the tree (BE-model) and the centrifugal order of the segment (S-model) as

$$p_i = C2^{-S\gamma}B/Nn_i^E, \quad (7)$$

with γ denoting the centrifugal order of the terminal segment and $C = n/\sum_{j=1}^{n} 2^{-S\gamma_j}$ being a normalization constant, with a summation over all n terminal segments. The normalization ensures that the summed branching probability per time-bin of all the terminal segments in the tree does not change. The growth rate will not be changed either under such condition and will still be determined solely by the parameters B and E. For S = 0 the order dependency in the branching probabilities disappears and the BES-model reduces to the BE-model with $p_i = B/Nn_i^E$.

Thus, the BES-model combines the properties of the BE-model in generating the variation in the number of terminal segments and the properties of the QS-model (with Q taken to be zero) by generating realistic variations among topological tree types. Because the latter variation has been extensively discussed in previous papers (e.g., see Van Pelt et al., 1992), we will ignore this variation in the present study and focus only on the variation in the number of terminal segments in the observed dendritic data sets. Then, it suffices to use the BE-model.

The BES-model has been defined on a time-bin scale without the need of specifying the actual durations of the different time-bins. These durations become important, however, when we wish to correctly describe the time-course of the (mean) number of terminal segments per dendritic tree during development. This final extension of the model will be described later, following a test of the BE-model against observed dendritic trees.

Simulation procedure

The simulation of the growth process for the general BES-growth model proceeds according to the following algorithm. For a given tree at a given time-bin, the branching probabilities are calculated for all of the n terminal segments with, for S ≠ 0, the centrifugal order γ being taken into account of each of them. Then, using a uniform random number between 0 and 1, it is decided for each terminal segment whether a branching event actually occurs in the given time-bin (i.e., a branching event occurs when the random number is smaller than or equal to the branching probability for that segment). A branching event implies that a new terminal segment is attached to the branching segment. When none of the segments have branched, the tree maintains its structure into the next time-bin. The process starts at the first time-bin with a single (root) segment and stops at the last time-bin. Note, that the number of time-bins is arbitrarily chosen, but such that the branching probability per time-bin is much smaller than unity.

Comparison of the shapes of the observed and the BE-model-predicted degree distributions

Two methods have been used for finding the optimal values for the parameters B and E for a given set of observed dendrites. In the moment method the (mean, sd) values of the observed degree distribution are plotted as a data point in the parameter map (Fig. 4) and the corresponding B and E values are derived from the position of this point in the (B, E) parameter grid. The shape of the model degree distribution, calculated for these model parameters, is subsequently tested against the shape of the observed distribution by means of the χ^2 test. In the maximum likelihood method (MLE) the B and E parameter values are estimated by optimizing the shape of the model distribution to the observed distribution by means of a maximum likelihood procedure. For general information concerning maximum likelihood estimators the reader is referred to Cox and Hinkley (1974) and for a specific application to Verwer et al. (1987).

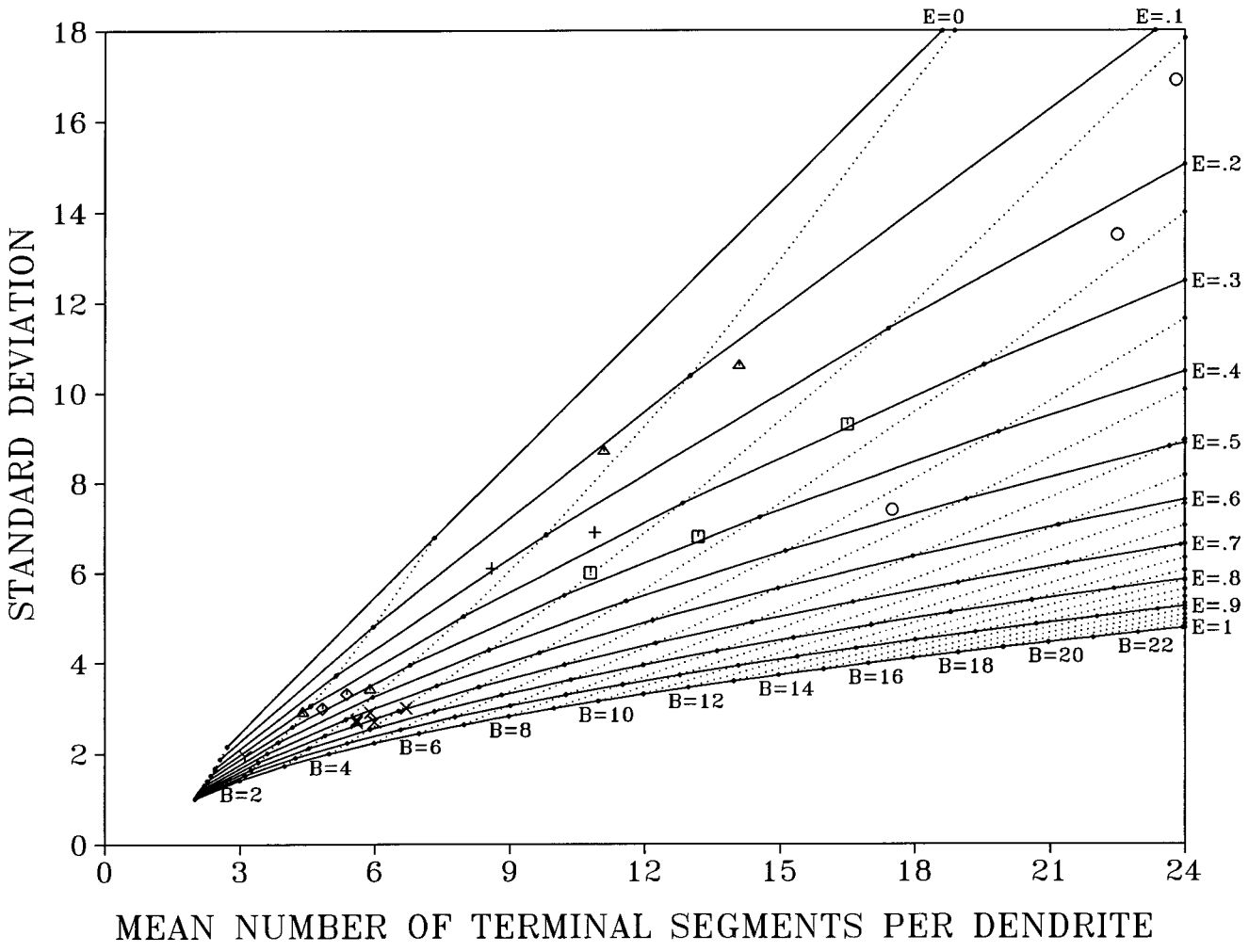

Fig. 4. Mapping of the (B, E) parameter grid onto the (mean,sd)-plane. The map is obtained by calculating for many pairs of (B, E) growth model parameter values the mean and standard deviation of the degree distribution, produced by the model, which are subsequently plotted as a point in the (mean,sd)-plane. The continuous lines connect points in the (mean,sd)-plane with equal E value, the dotted lines connect points with equal B value. The observed data points from Table 1 are plotted according to their mean and sd values and labeled as square (cat motoneurons), circle (frog motoneurons), triangle (rat motoneurons), plus sign (cultured cholinergic interneurons), times sign (rat pyramidal neurons), Y (rat multipolar nonpyramidal neurons), and diamond (human dentate granule cells).

RESULTS OF BE-MODEL

Comparison of observed and calculated degree distributions

Optimal values for the model parameters B and E for the different cell types are obtained using the moment method (Table 1, columns 5 and 6) and the MLE method (Table 1, columns 10 and 11). The mean's and standard deviation's of the calculated degree distributions for these parameter values are given in columns 7 and 8 for the moment method outcomes, and in columns 12 and 13 for the MLE outcomes. The levels of significance of the χ^2 tests in Table 1, all being larger than 0.05, demonstrate that the model distributions are not significantly different from the observed ones. The (B, E) model is thus able to accurately describe the shape of all the observed degree distributions. The goodness-of-fit is also qualitatively demonstrated in Figure 5 with the observed distributions plotted as continuous lines and the best-fitting model distributions (from the moment method) by dashed lines. Also the mean's and sd's of the observed distributions are accurately reproduced by the model. The mean difference between the estimates by both methods was found to be -0.012 (sd = 0.124) for parameter B and -0.006 (sd = 0.025) for parameter E.

Relationship between model parameters. To determine how the optimal parameters B and E correlate with the mean and sd of the degree distributions, two-way scatterplots have been made of these quantities (Fig. 6). The correlation coefficients, given in the heading of each panel, reveal significant correlations between sd and mean, between B and both mean and sd, and between E and both mean and sd. No correlation was found between B and E, indicating that these parameters are independent, and suggesting that they reflect different factors regulating dendritic complexity.

Complexity and variability of dendrites. The question is further addressed whether different classes of neurons can be distinguished on the basis of their degree

TABLE 1. Comparison of Observed and Model Predicted Distributions of the Number of Terminal Segments in Dendritic Trees[1]

Observations				Model best fit outcomes									
				Moment method					MLE method				
		Degree				Degree					Degree		
Cell types	n	Mn	Sd	B	E	Mn	Sd	χ^2-test p-value	B	E	Mn	Sd	χ^2-test p-value
Cat motoneurons													
Cullheim et al. (1987)													
Gastrocnemius-Fast	44	16.5	9.3	4.55	0.29	16.6	9.4	0.33	4.4	0.27	16.6	9.5	0.31
Soleus-Slow	10	10.8	6.0	3.95	0.36	10.8	6.0	0.17	4.5	0.39	12.5	6.4	0.23
Frog motoneurons													
Birinyi et al. (1992)													
Rana esc.-Lumbar	25	23.8	16.9	4.15	0.14	23.8	16.8	0.09	4.0	0.12	24.4	17.2	0.21
Rana esc.-Brachial	17	17.5	7.4	6.35	0.47	17.7	7.5	0.37	6.2	0.46	17.7	7.4	0.44
Babalian and Chmykhova (1987)													
Rana rid.-Lumbar	33	22.5	13.5	4.75	0.23	22.4	13.3	0.19	4.9	0.24	23.4	13.3	0.16
Rat motoneurons													
Chmykhova et al. (1987)													
Young Lumb. DLN	29	5.9	3.4	2.75	0.43	5.8	3.4	0.48	2.9	0.47	6.0	3.3	0.25
Young Lumb. VLN	27	11.1	8.7	2.85	0.11	11.1	8.7	0.14	2.9	0.13	11.1	8.3	0.31
Chen and Wolpaw (1994)													
Adult triceps surae	104	14.1	10.6	3.25	0.13	13.9	10.4	0.34	3.3	0.14	14.1	10.1	0.34
Ulrich et al. (1994)													
In culture	35	4.4	2.9	1.95	0.31	4.4	2.9	0.65	2.0	0.33	4.4	2.9	0.41
Rat cholinergic interneurons													
In culture, Studer et al. (1994)													
No NGF	58	8.6	6.1	2.75	0.19	8.5	6.1	0.48	3.0	0.26	8.5	5.5	0.39
With NGF	59	10.9	6.9	3.45	0.26	10.8	6.9	0.07	3.5	0.27	10.9	6.7	0.15
Rat pyramidal neurons													
Uylings et al. (1990)													
L 2/3 30 days	413	5.6	2.68	3.35	0.68	5.4	2.6	0.24	3.40	0.68	5.6	2.6	0.62
L 2/3 150 days	494	5.6	2.74	3.25	0.66	5.5	2.7	0.12	3.35	0.67	5.6	2.7	0.33
Larkman et al. (1993)													
L2/3	78	6.7	3.0	4.05	0.69	6.7	3.0	0.33	4.10	0.69	6.7	3.0	0.36
Thick L5	65	6.0	2.7	3.85	0.74	6.0	2.7	0.55	3.75	0.71	6.0	2.7	0.81
Slender L5	44	5.9	2.9	3.35	0.63	5.8	2.9	0.62	3.30	0.61	5.9	2.9	0.60
Rat multipolar nonpyramidal neurons													
Uylings et al. (1990)													
150 days	532	3.1	1.9	1.49	0.42	3.1	1.9	0.91	1.55	0.45	3.1	1.9	0.97
Rat purkinje cells													
Woldenberg et al. (1993)													
1 month	9	455	42	60.0	0.585	448	41.4	0.22					
10 months	23	579	91										
18 months	25	409	125										
28 months	22	499	74										
Berry and Bradley (1976)													
5 days	17	60	21										
10 days	17	79	22										
15 days	10	245	74										
30 days	10	477	58	40	0.486	482	58						
50 days	10	543	144										
Human dentate granule neurons													
De Ruiter and Uylings (1987)													
Aged controls	167	4.8	3.0	2.27	0.39	4.8	3.0	0.91	2.25	0.37	4.8	3.0	0.50
Mrzljak and Uylings (unpubl)													
Adult	43	5.5	3.3	2.44	0.37	5.4	3.3	0.76	2.45	0.35	5.5	3.3	0.81

[1]Results of the analysis of experimental degree distributions. Column 1 contains the references for the used neuronal data sets, see also the text. Column 2 contains the number of dendrites in the data set. Column 3 and 4 contain the means and standard deviations, respectively, of the degree distributions of the observed dendritic trees. Model results, optimized by means of the Moment Method, are given in Columns 5–9 and optimized by the MLE method given in columns 10–14. Columns 5, 6, 10, and 11 contain the values for the parameters B and E that let the growth model optimally describe the shape of the observed distributions. The means and standard deviations of these modelled distributions are given in columns 7–8 and 12–13, respectively. A χ^2-test is used to compare the shapes of the modelled and observed degree distributions, with the levels of significance given in columns 9 and 14. Rat Purkinje cells were analyzed by means of the Moment Method only, because experimental data of the shape of the degree distribution were not available. For reasons given in the paper, only the 1 month data is analyzed.
n, number of dendrites; DLN, dorsal lateral nucleus; VLN, ventral lateral nucleus; NGF, nerve growth factor; Mn, mean; Sd, standard deviation; MLE, maximum likelihood estimate; L, cortical layer.

distributions. The scatterplot in Figure 6B shows a strong clustering of (B, E) values of the five pyramidal cell groups around their mean point [$\overline{B}$(sem), $\overline{E}$(sem) = 3.55(0.17), 0.68(0.02)]. Both the motoneuron dendrites of cat (□), rat (△), and frog (⊙), with mean values [$\overline{B}$(sem), $\overline{E}$(sem) = 3.92(0.4), 0.29(0.04)], the rat multipolar nonpyramidal cells (Y) with (B, E) = (1.49, 0.42) and the human dentate granule cells (◇) with ($\overline{B}$, $\overline{E}$) = (2.36, 0.38) appear to differ significantly from the rat pyramidal cells (×) with respect to $\overline{E}$. Rat Purkinje cell groups (not displayed in the figure) with ($\overline{B}$, $\overline{E}$) = (50,0.54) differ significantly from all other cell types with respect to $\overline{B}$, while for $\overline{E}$ they fall between the pyramidal cells and the other cell types.

Course of mean and standard deviation of degree distribution versus time-bin number

The shapes of the degree distributions are obtained by means of the recurrent equation, specified in the Appendix, which is based on the calculation of the distribution at all successive time-bins. How the mean and sd develops versus time-bin is illustrated in Figure 7A, in which the time course is calculated for the pyramidal cell basal dendrites, by using their mean ($\overline{B}$, $\overline{E}$) = (3.55, 0.68) values. Knowing the time course of the mean degree $\overline{n}_i$ as a function of time-bin number i, the averaged branching probability per terminal segment per time-bin can be

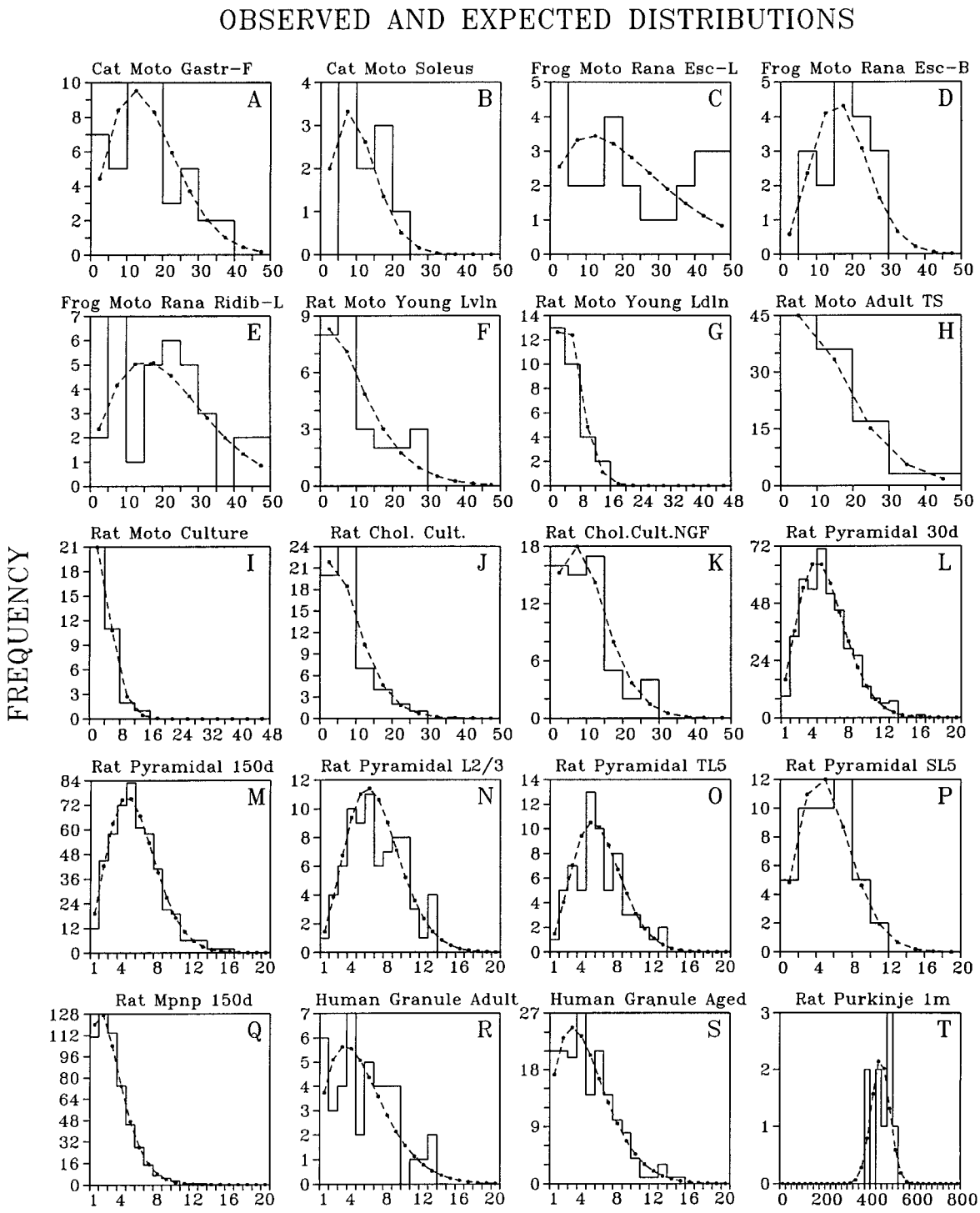

Fig. 5. Frequency distributions of the number of terminal segments per dendritic tree for different cell types and species, as indicated in the headings of the panels. Each panel displays the observed frequency distribution, plotted as a continuous line histogram, and the expected distribution for the optimized growth model, plotted by a dashed curve. The values for the mean and standard deviation of the observed and expected distributions, as well as the optimized model parameters B and E are given in Table 1. A full list of references and sources of the unpublished data is given in Materials and Methods. Note that in many of the distributions the classes of the number of terminal segments have been lumped, in order to obtain a sufficient number of observations per class. For instance, the range of 1–52 terminal segments in panel I is divided into 13 classes, with trees with 1–4 terminal segments counted in class 1, with 5–8 terminal segments into class 2, etc. Lumping was not applied in the distributions in the panels L–O and Q–S. The figure demonstrates i) the large variation in the number of terminal segments per dendritic tree, ii) the differences in shapes of the terminal segment number distribution between different cell types and species, and iii) the accuracy with which the optimized growth model can reproduce the shapes of the observed distributions. Gastr-F, gastrocnemuis-Fast; Esc-L, esculenta-lumbar; Esc-B, esculenta-brachial; Ridib-L, ridibunda-lumbar; Lvln, lumbar ventral lateral nucleus; Ldln, lumbar dorsal lateral nucleus; TS, triceps surae; Chol, cholinergic; TL5, thick layer V; SL5, slender layer V; Mpnp, Multipolar nonpyramidal.

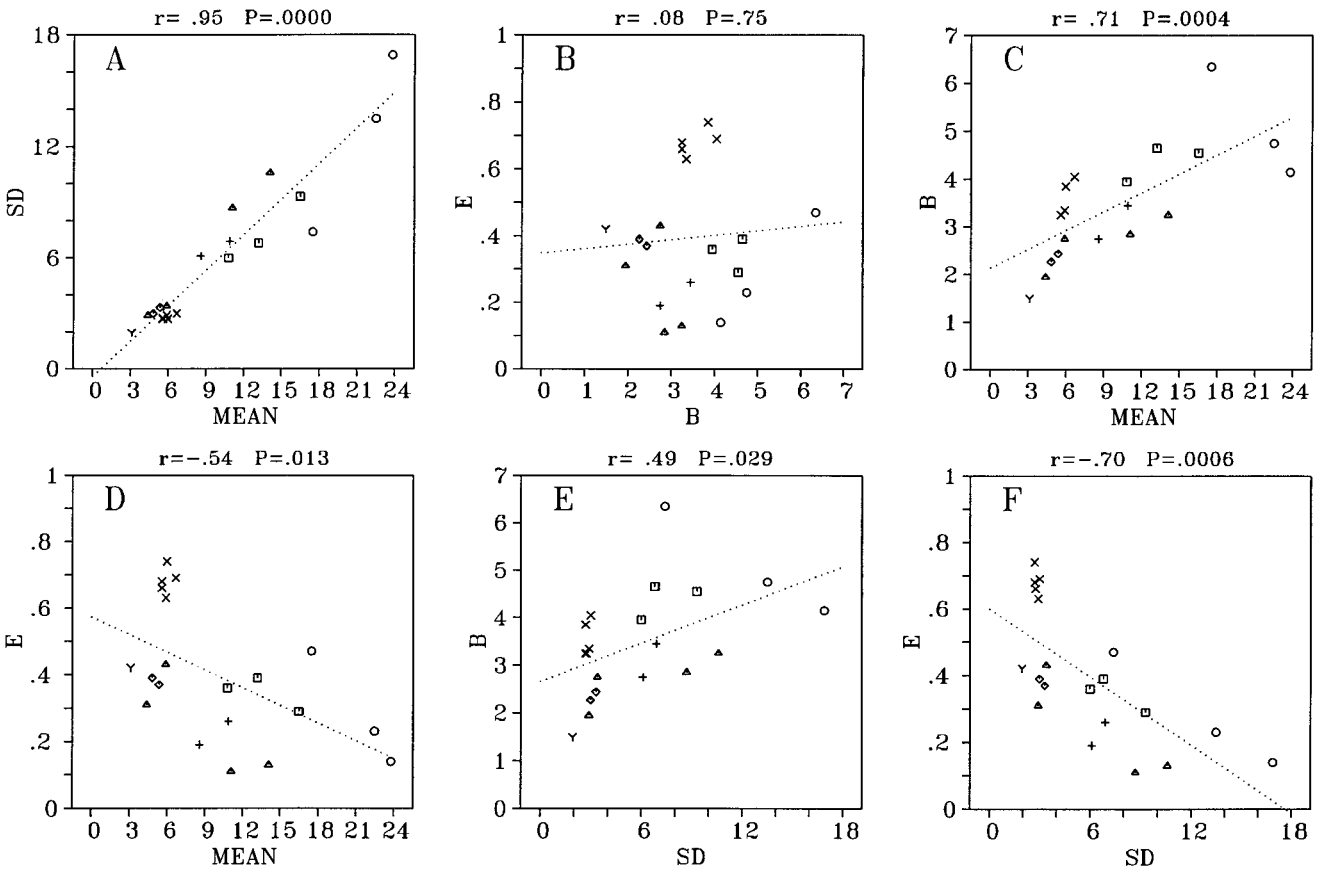

Fig. 6. Scatterplots of the outcomes of the analysed data sets (frequency distributions of the number of terminal segments per dendrite) listed in Table 1. Scatterplots are given for the six combinations of the mean and standard deviation of the observed distribution and the optimal growth model parameter B and E. The dotted line indicates the linear regression through the data points. In the heading of each panel is given the coefficient of correlation r and the level of significance P. The symbols refer to the different classes of neurons (like in Fig. 4) as square (cat motoneurons), circle (frog motoneurons), triangle (rat motoneurons), plus sign (cultured cholinergic interneurons), times sign (rat pyramidal neurons), Y (rat multipolar nonpyramidal neurons), and diamond (human dentate granule cells). Note the absence of correlation in the B-E scatterplot in panel B (i.e., $P = 0.75$). The Purkinje cell data points are outside the scale of the panels.

calculated using Eq. 5 ($p_i = B/N\overline{n_i^E}$). Its course vs. time-bin number is displayed in Fig. 7B. Similar courses for the mean and sd, and the branching probability vs. time-bin for the 1 month Purkinje cell group of Woldenberg et al. (1993) are given in Figure 7C,D, respectively. They are calculated for the values (B, E) = (60, 0.585). The growth courses of the mean appear to be non-linear functions of time-bin number with an increasing growth rate. The branching probabilities show a declining pattern versus time-bin number. These patterns illustrate how, because of the nonzero value of E, the increasing number of terminal segments has a reducing effect on the branching probabilities. The increasing growth rate, however, demonstrates that this reduction does not fully compensate for the increase in the terminal segments. As can be derived from Eq. 6 ($\overline{\Delta n_i} = Bn_i^{1-E}/N$), a decreasing growth rate per time-bin will occur for values of E larger than one. For all the analyzed data sets, however, the optimum E-values appear to be smaller than one.

Expected branching probabilities per unit of time

Branching probabilities have so far been defined per time-bin via the parameters B and E, optimized such that the model degree distribution at the last time-bin corresponds as closely as possible to the observed one. No assumptions were made for the durations of the different time-bins, but to describe the branching process in real time, we will need to make the time-bin durations explicit. The branching probability per time-bin p_i can then be transformed into a branching probability per unit of time p(t) via $p(t) = p_i/T_i$, with T_i the duration of time-bin i and p_i given by Eq. 5 ($p_i = B/N\overline{n_i^E}$). The growth rate per time-bin $\overline{\Delta n_i}$ is then transformed into a growth rate per unit of time via $dn/dt = \overline{\Delta n_i}/T_i$.

Equal time-bin durations. When all the time-bins T_i have equal durations, $T_i = T/N$, we obtain for the branching probability per unit of time $p(t) = Bn(t)^{-E}/T$, and for the growth rate $dn/dt = Bn(t)^{1-E}/T$. For values of E between 0 and 1, as found for the analysed data sets, the branching probability per unit of time is a monotonically decreasing function, while growth rate is a monotonically increasing function of time. Because of the linear transformation the continuous time functions have the same shape as the time-bin functions, for instance, as given in Figure 7A–D. Growth terminates eventually and one expect the growth function to stabilize at a constant value, and both the branching probability and the growth rate to go to zero

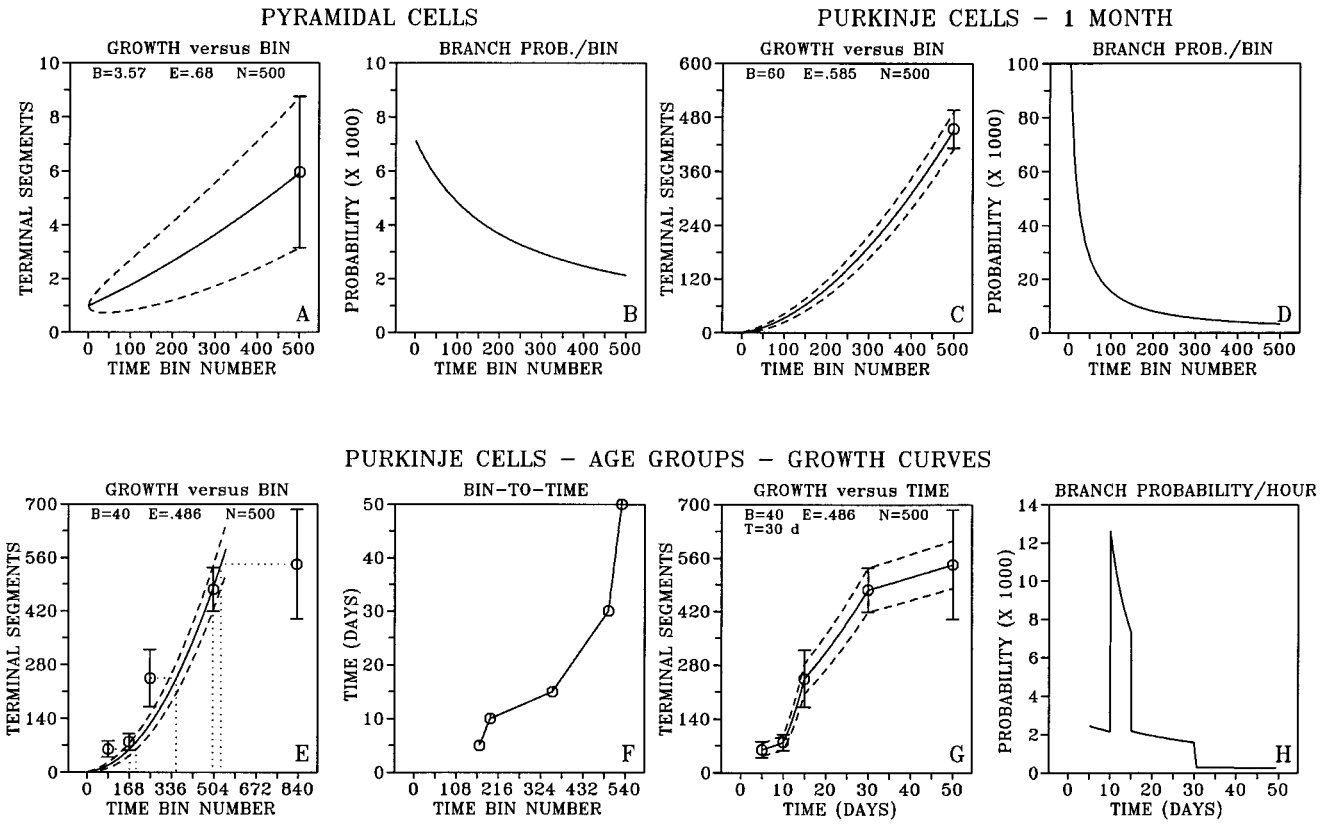

Fig. 7. Course of the mean and standard deviation of the degree distribution versus time-bin (growth curves), calculated with model parameters optimized for (**A**) the pyramidal cells and (**C**) the 1 month Purkinje cells. The corresponding branching probabilities per time-bin are given in (**B**) and (**D**), respectively. The model growth curves for the 30 days (post natal) old Purkinje cells is given in **E** in which also the observed means and standard deviations are plotted of the different age groups of Berry and Bradley (1976), by using a linear time scale with bin 500 corresponding with age of 30 days. The bin numbers at which the growth curve attains similar mean values as the data points are plotted in **F** against the age of the groups. **G** is obtained when the bin scale of panel (E) is transformed into a time scale using the bin-to-time curve in panel (F). **H** displays the branching probabilities per terminal segment per hour, calculated from the time course of the mean in G.

values. This is clearly not the case for the mentioned curves. The continuous curves in Figure 7A,C increase in values and in their derivatives with time-bin number, while the curves in 7B,D, although declining, do not converge to zero values. We shall therefore relax the condition of equal time-bin durations.

Unequal time-bin durations (BEST-model). Realistic growth curves can be estimated when degree distributions are available at several age points during development. Berry and Bradley (1976) have reconstructed Purkinje cell dendritic trees at five different age points and found mean(sd) values of the degree distributions of 60(21), 79(22), 245(74), 477(58), and 543(144) at days 5, 10, 15, 30, and 50, respectively [Berry and Bradley (1976), values estimated from Fig. 11; see also Woldenberg et al. (1993), p. 421]. The mean(sd) value at day 30 compares well with the 1 month outcome of 455(42) from the work of Woldenberg et al., (1993). These five data points from Berry and Bradley (1976) are drawn in Figure 7E using a linear time scale versus time-bin, such that time-bin N = 500 corresponds to real time T = 30 days. For the 30 days age group the optimal parameter values were found to be (B, E) = (40, 0.486), and the growth curve for these parameter values has also been drawn in Figure 7E. The observed growth curve deviates clearly from the one calculated on the basis of equal time-bin durations.

The model growth curve can be brought into accordance with the observed data points by defining appropriate (unequal) values for the time-bin durations. The following procedure has been applied. By using the model growth curve (optimized for the 30 day age group), the bin number for each of the other age groups was calculated at which the theoretical growth curve attained corresponding values for the observed mean. This is shown in Figure 7E by the dotted lines, drawn horizontally from the observed data points towards the growth curve, and from the intersection points vertically to the bin number axis. In this way, the age of a Purkinje cell group can be associated with a particular bin number. The outcomes for the five cell groups are subsequently plotted as data points in Figure 7F. A bin-to-time mapping was next obtained by interpolating between these data points in a, for simplicity, linear manner. The bin-to-time curve in Figure 7F clearly deviates from the straight line, which would be expected when all the time-bins have an equal duration. The bin durations, determined by the slope of the curve, increase with time-bin number between the 2nd and 5th data point. No assumptions have been made concerning the time of onset

of branching, i.e., the time of the first bin. Therefore, the first part of the bin-to-time curve has not been drawn.

By using this bin-to-time function, the time-bin scale of Figure 7E was transformed into a time scale resulting in a model growth curve of the mean versus time (Fig. 7G) that passes through the observed data points. Note, that by this bin-to-time transformation the relationship between mean and sd of the model curve is not changed. Finally, the time course of the branching probability per terminal segment per unit of time was calculated, by using the time-bin durations derived from the bin-to-time curve (Fig. 7H). It shows that the branching probability per hour of a terminal segment has a value of about 0.0023 (i.e., 0.06/day) between days 5 and 10, rapidly increases to a value between 0.008 and 0.013 (i.e., 0.2–0.3/day) between days 10 and 15, and then drops back to about 0.002 (i.e., 0.05/day) between days 15 and 30 before a final decline to about 0.0003 (i.e., 0.007/day). The sharp transitions in the curve originate from the piece-wise linear approximation of the bin-to-time function. Nevertheless, with the data shown in Figure 7, an estimate is obtained for the absolute values of the branching probabilities per terminal segment per hour. Striking is the increased branching probability in the Purkinje cells between day 10 and 15, while before and after this transient increase the probabilities are more or less stable at a level of about 0.002 per hour. This peak coincides with the period of largest growth rate in terminal segment number (day 10–15) (see Fig. 7G and Table 1). The model growth curve in Figure 7G is optimized to reproduce the observed mean(sd) at day 30 and to run correctly through the observed means of all age groups. Figure 7G demonstrates that the observed sd's at day 5 and 10 also correspond closely with the sd's of this growth curve, but at days 15 and 50 are larger then predicted.

In a similar way, the developmental course of branching probabilities can be estimated for other cell types when dendritic data sets are available at different points in time during development. We are presently analysing data sets of developing rat cortical pyramidal and nonpyramidal dendrites (Uylings et al., 1994). Based on the developmental curves of the total number of basal dendritic segments per cell and of segment length and total dendritic length, these authors concluded that the phase of rapid dendritic growth ends at about postnatal day 18.

DISCUSSION

Agreement between experimental and theoretical data

The model-based study of the distribution of the number of terminal segments in dendritic trees has demonstrated that the large variation observed in the number of terminal segments per dendrite (i.e., degree) can emerge naturally from the stochastic behavior of branching growth cones. By dividing the developmental period into a series of time-bins, it turns out that a constant branching probability per time-bin results in unrealistic distributions for the number of terminal segment per dendritic tree. In contrast, the observed degree distributions could be accurately reproduced when the branching probability per time-bin was made to decrease with increasing number of terminal segments in a growing tree. Only two parameters (B and E, see Eq. 5) were needed in the model to obtain this result. Two different methods have been used for estimating optimal parameter values, viz., the moment method for approximating the mean and sd of the observed degree distribution, and the maximum likelihood method for approximating the shape of the degree distribution. The fact that similar results were obtained demonstrates the reliability of the estimates. Because the shape of any distribution is determined by many more than the first two moments, a good fit means that the model is not just descriptive but also has "explanatory" value, i.e., by explaining correctly the higher-order moments. Since the model is simple in structure, based only on randomness and degree-dependent branching probabilities, it may appear surprising that the natural variation in the number of terminal segments per dendrite can be so accurately generated, but random branching had already been shown to be a sufficient condition for explaining topological variability in dendritic shapes (Van Pelt et al., 1992, Dityatev et al., 1995). Randomness in branching behavior could originate from the many factors involved in the splitting of growth cones: the dynamic behavior of filopodia in sensing highly variable local environmental cues, their interaction with the actin cytoskeleton, and the dynamic instability of the assembling/disassembling microtubule cytoskeleton seem to be major components herein (e.g., Martin et al., 1993; Kater et al., 1994; Letourneau et al., 1994; Van Veen and Van Pelt, 1994).

The formulation of the branching process on a series of time-bins still leaves the freedom to define the durations and to map the time-bins on a real time scale. Such mapping does not interfere with the model's ability to predict the correct degree distribution and thus mean/sd relationships. It is shown that equal time-bin durations result in an increasing growth rate of the mean number of terminal segments per dendrite. It is demonstrated how to obtain a bin-to-time transformation such that the model growth curve for the mean passes through the observed data points for different age groups.

An important feature of the model is that it relates the time course of the mean and sd of the degree distribution with the branching probabilities of the growth cones per unit of time. From the Purkinje cell age groups the branching probability per day can be estimated to have a value of the order of 0.05 between day 5 and day 30 with a transient increase to a level of about 0.2–0.3 between day 10 and 15. Although the piece-wise linear approximation may seem unrealistic, a more smoothed version is not expected to change the order of magnitude of the derived branching probabilities. Alternatively, a smoother growth curve can be obtained when experimental data become available for more age points. Evidently, given the small number of age points for the rat Purkinje cells, the estimated branching probabilities per unit of time are solely predictions from the model, and still needs to be tested experimentally. When only a single group at one developmental stage is available, such as the cortical pyramidal cells in this study, the time course of the branching probabilities can only be estimated if assumptions are made with respect to the time-bin durations. It should be noted that the estimation of branching probabilities is obtained from different cell groups at different ages, and not from longitudinal studies on the same cells, (e.g., Uylings et al., 1994).

Termination of growth

Growth rate is a function of both the branching probability of terminal segments per unit of time and the number

of terminal segments. Growth terminates when the decline in branching probability per unit of time exceeds the increase in terminal segment number. Such a decline is achieved by increasing the durations of the time-bins, i.e., by choosing an appropriate time-bin duration function. This is shown in the analysis of the Purkinje cell age groups in which the reduction in growth rate and the stabilization of the growth curve (Fig. 7G) could be obtained by increasing the durations of time-bins (steeper slope in Fig. 7F).

Interpretation of parameters

Three aspects have been distinguished in dendritic branching by the model, viz., i) the "basic" branching process of an individual growth cone, defined by the expected number of branching events B during the developmental period under (hypothetical) isolated conditions, ii) the "proliferation" of the number of growth cones in the growing tree, and iii) the "modulation" of the "basic" branching probability by the increasing number of growth cones (determined by the parameter E). The lack of correlation between B and E in the analyzed data sets indeed suggest that aspects i and iii reflect different mechanisms in dendritic branching. All three aspects finally determine the shape of the terminal segment number distribution, with B significantly correlating positively, and E correlating negatively with both mean and sd. An interesting question concerns the mechanisms underlying iii, the "modulation" effect. It could be a competition effect between growth cones when the drop in branching probability is a direct consequence of an increase in their number of terminal segments (for instance, because of the limited availability of a critical substance). Alternatively, it might simply be a phenomenon of decreasing branching probability with age, in which case there will be a correlation with an increasing number of terminal segments.

Parameters B and E may both represent important cell-type specific mechanisms in growth-cone branching, as they show a strong clustering per cell type in the B-E parameter plane (see Table 1 and Fig. 6). Parameter E discriminates significantly between rat pyramidal basal dendrites (with $\overline{E}$(sem) = 0.68(0.02)) and other neuron classes [for motoneurons $\overline{E}$(sem) = 0.29(0.04), for multipolar nonpyramidal cells E= 0.42, and for human dentate granule cells E = 0.38]. The larger value of E for the pyramidal cells suggests that during outgrowth of their dendrites the branching probabilities decline stronger with increasing number of terminal segments than in the other neurons.

In a recent study, Burke et al. (1992) have searched for a parsimonious description of motoneuron morphology by using computer simulations based upon empirically measured distribution functions for several morphological parameters, including the lengths and diameters of dendritic branches. Such a description was given in terms of probability functions needed for the stochastic reconstruction of the dendrites, and "included two processes, one for generating (the length of) individual branches, given their proximal diameters, and the second for selecting proximal diameters for the daughter branches produced at dichotomous branching points." The branching probability (i.e., the probability of having a bifurcation point per unit length of the segment) was found to depend strongly on the diameter of branches, with a weaker negative dependence on distance from the root. Daughter branches have smaller diameters than their parents so that the decrease in branching probability applies for branches of increasing branch order. These branches will have been formed later in development, such that the decrease in branching probabilities coincides with an increasing number of terminal segments. Although the structure of this model and the meaning of the probabilities differ from the present model (formulated as a process in time) this outcome is nevertheless in good agreement with the present findings.

A completely different approach in reconstructing dendritic trees by a stochastic rule has been developed by Kliemann (1987) and recently used by Carriquiry et al. (1992) and Uemura et al. (1995). Trees are reconstructed on the basis of splitting probabilities, indicating for each centrifugal order the probability whether a segment will end in a bifurcation point or in a terminal tip. The splitting probabilities are obtained from the ratios of the number of segments of successive orders summed over all the trees in the data set. The random trees generated by this method appeared to have realistic variation in their shapes. This procedure requires as many parameters as there are centrifugal orders in the data set, which have to be estimated for each new group of dendrites under consideration.

Propagation of uncertainties in mean(sd) into uncertainties in estimated B, E values

Because of the particular line pattern in the mapping of (mean,sd) space onto (B, E) space (Fig. 4), uncertainties in both mean and sd propagate differentially into correlated uncertainties in B and E. An illustration of this effect is given by the outcomes of the 1 month Purkinje cell groups of Berry and Bradley (1976) with mean(sd) = 477(58) and (B, E) = (40, 0.486) and of Woldenberg et al. (1993) with mean(sd) = 455(42) and (B, E) = (60, 0.585). The different outcomes for B and E are mainly caused by the relatively small difference in sd.

Growth and regression

In the present model, only growth by branching was considered. Although dendritic regression, accompanied by the loss of branches, might not effect the estimates of the Q,S parameters under random pruning conditions (Van Pelt, 1997), it will certainly influence the mean and sd of the degree distributions. Loss of branches is a prominent phenomenon during cerebellar Purkinje cell dendritic development in rats. Woldenberg et al. (1993) showed that the number of segments increases up to 10 months, declines at 18 months, and increases again at 28 months. They also noted that at 10 and at 28 months and even more so at 18 months, the population consisted of one group with a small, and another with a large number of segments, suggesting the coexistence of declining and growing cells. That this coincidence of growth and decline leads to a broadening of the degree distribution is clearly demonstrated by the larger sd values for the 10, 18, and 28 month groups in comparison with the 1 month group (Table 1). For this reason the BE model has been applied only to the 1 month group, as having recently experienced a period of maximal growth, and for which the mean and sd of the degree distribution have been determined primarily by the growth process, and not "disturbed" secondary by dendritic regression.

In a study of the postnatal development of dendrites of cat triceps surae motoneurons, Ulfhake et al. (1988) and

Ulfhake and Cullheim (1988) showed that the mean number of terminal segments per dendrite remained constant over the full postnatal period up to adulthood. Also the minimal and maximal values of the observed degree distribution appeared to be very similar during the postnatal development. Nevertheless, topological analysis suggested a transient phase of remodeling in the 2nd and 4th postnatal week, involving collateral outgrowth and resorption of peripheral dendritic branches. Thus, the primary branching process seems to be finished already at birth, with a modest remodeling phase some weeks later, not impairing the mean and extremes of the degree distribution. Apart from the branching pattern, age effects were clearly present in the elongation of the (mainly terminal) segments from birth to 6 weeks of age.

A clear remodeling phase was found by Núñez-Abades et al. (1994) in the morphological development of rat genioglossal motoneurons studied in vitro. A "simplification" of the dendritic tree in the first period from birth to 13–15 days involved a significant decrease in the number of terminal endings and thus number of branches per dendrite. This phase was followed by a period of re-elaboration by collateral outgrowth producing trees, similar in configuration to the newborn ones. The remodeling process resulted also in a transient increase in the symmetry of the trees.

Model approach

The mathematical model approach has shown to be an essential tool in studying the proliferation in the number of segments during dendritic outgrowth and the variation in finally formed dendrites. It has revealed unexpected differences among neuronal cell types and it allows the estimation of growth-cone branching probabilities per unit of time. It further allows explicit testing of hypotheses about dendritic development, and offers greatly improved tools for extracting information from dendritic branching patterns, which are generally obtained via a time-consuming process of morphological reconstruction. The model approach should fruitfully complement in vivo studies of growth cone behavior and development of dendritic morphology, which are seriously hampered by the difficulty of capturing the dynamics of growth (e.g., Ulfhake and Cullheim, 1988).

The growth model describes dendritic growth as a stochastic branching process and has shown to result in realistic segment number variations for a variety of neuronal cell types and species, as observed in snapshot data at one or a few age points, as well as for the growth curve through these data points (fit). This result was obtained by choosing an appropriate nonlinear transformation of the time scale, thus implying a modulation of the branching probabilities per unit of time of single terminal segments. Although a minimal set of growth rules appears to be sufficient, this does not mean that the actual growth processes must have behaved as such. Other, presumably more complex, growth patterns could in principle result in similar segment number distributions. The growth model presented here assumes that the rules for branching (equations for the branching probabilities) and the values of the parameters B, E, and S remain constant during the growth process. Actual dendritic development, of course, could deviate considerably from such a stationary process.

The structure of the present growth model, describing dendritic development as a process in time, makes it possible to include such non-stationarities. Such a situation could occur, for instance, during phases of remodeling. Branching might then become differentiated in different areas of the dendrite, implicating a changed dependence on centrifugal order (and thus changes in parameter S). In a recent study on the impact of pruning and variable growth rules, Van Pelt (1997) showed that non-stationarity in the dependence on centrifugal order results in an increase in topological variation. When remodeling is a persistent and prominent phenomenon during dendritic growth, such an increase may indeed be expected. A net loss of branches may be described by including a pruning process, as for instance described in Van Pelt (1997). Changes in the way in which branching probabilities depend on the total number of segments via parameter E may also be not constant as is assumed in the present model. This will presumably influence the mean/sd relationship in the final segment number distribution. Such changes can be accounted for by defining parameter E as a function of time. How such a function can be estimated from degree distributions, available for only a few age classes, has not been worked out in this study, but is subject of present research.

The accurate description of the topological and segment number variation in dendritic trees by the present model implicates that any measure, which is dependent on the number and the position of segments in the tree can be reproduced accurately by the BES-model. This property was further verified for the measures maximum order and mean order, indicating the maximal centrifugal order of the segments in a tree, and the mean centrifugal order, respectively. To this end, trees were simulated using B, E, and S parameters derived from the observed dendritic data sets and the mean(sd) values of the parameters degree, tree asymmetry index, maximum order, and mean order were calculated. No significant differences ($P > 0.05$) were found between the model-generated and the actually observed dendrites.

The main goal of the ongoing modeling work of dendritic growth is to understand how characteristic dendritic morphologies can emerge from the dynamic behavior of growth cones, and to test the extent to which variations, observed in different cell types could arise from stochasticity in growth cone behavior. To this end, also the metrical properties of dendritic trees (viz. length of segments, which show substantial variations; e.g., Hillman, 1979, 1988; Uylings et al., 1989, Burke et al., 1992) will need to be included, which is the subject of ongoing investigation. When successful, the model's ability to generate model dendrites with realistic morphological properties will also be relevant in studies of the possible functional implications of structural variation among dendrites of a given type. Especially in the field of computational neuroscience, substantial progress has been made in modeling bioelectric phenomena (e.g., membrane potentials, firing behavior) in neurons to a high degree of spatial and temporal accuracy (e.g., Rall et al., 1992; Segev, 1992; De Schutter and Bower, 1994a,b; Traub and Jefferys, 1994; Schierwagen, 1994). These studies have so far been performed on a limited number of accurately reconstructed neuronal morphologies, but for a good assessment of the impact of morphological variability on bioelectric properties, methods for generating sets of model neurons with realistic variations in their shapes are needed. The present study

contributes to this goal with respect to the variation in the number of terminal segments per dendrite.

In conclusion, a model is obtained for the growth of dendritic branching patterns that accurately describes the variation found in these patterns. The assumptions in the BE-model result in a good description of the variation in the number of terminal segments per dendritic tree. The assumption of constant branching probabilities, independent of the number of segments in the tree (B-model), has been shown to give unrealistic results. Including a distinction of terminal segments for their centrifugal order position in the tree (BES-model) additionally gives a good description of the variation in topological tree types. The transformation of the time-bin scale into a time scale (BEST-model), by using dendritic data at several ages, makes it possible to obtain an estimate of the time course of the branching probabilities per unit of time.

APPENDIX

The distribution of the number of terminal segments in dendritic trees after a period of growth can be calculated by means of the recurrent expression

$$P(n, i) = \sum_{j=0}^{n/2} P(n - j, i - 1) \binom{n - j}{j} \cdot [p(n - j)]^j [1 - p(n - j)]^{n-2j}, \quad (8)$$

with P(n, i) denoting the probability of a tree of degree n at time bin i with P(1, 1) = 1, p(n) denoting the branching probability per time-bin of a terminal segment in a tree of degree n, with $p(n) = Bn^{-E}/N$. A tree of degree n at time-bin i emerges when j branching events occur at time-bin i − 1 in a tree of degree n − j. The recurrent equation expresses the probabilities of all these possible contributions from j = 0, . . . , n/2. The last two terms express the probability that, in a tree of degree n − j, j terminal segments will branch while the remaining n − 2j terminal segments will not do so. The combinatorial coefficient $\binom{n - j}{j}$ expresses the number of possible ways of selecting j terminal segments from the existing n − j ones.

ACKNOWLEDGMENTS

We are very grateful to Dr. G.J.A. Ramakers and especially to Dr. M.A. Corner for their critical comments and valuable suggestions. We thank the authors, listed in the Materials and Methods section, for allowing us to use their dendritic data.

LITERATURE CITED

Babalian, A.L., and N.M. Chmykhova (1987) Morphophysiological description of connections between single ventrolateral tract fibers and individual motoneurons in frog spinal cord. Brain Res. *407:*394–397.

Berry, M., and P. Bradley (1976) The growth of the dendritic trees of Purkinje cells in the cerebellum of the rat. Brain Res. *112:*1–35.

Birinyi, A., Antal, M., Wolf, E., and G. Szekely (1992) The extent of the dendritic tree and the number of synapses in the frog motoneuron. Eur. J. Neurosci. *4:*1003–1012.

Bray, D. (1992) Cytoskeletal basis of nerve axon growth. In P.C. Letourneau and S.B. Kater (eds): The Nerve Growth Cone. New York: Raven Press, pp. 7–17.

Burke, R.E., W.B. Marks, and B. Ulfhake (1992) A parsimonious description of motoneuron dendritic morphology using computer simulation. J. Neurosci. *12:*2403–2416.

Carriquiry, A.L., W.P. Ireland, W.H. Kliemann, and E. Uemura (1992) Statistical evaluations of dendritic branching patterns. Bull. Math. Biol. *53:*579–589.

Chen, X.Y., and J.R. Wolpaw (1994) Triceps surae motoneuron morphology in the rat: A quantitative light microscopic study. J. Comp. Neurol. *341:*1–5.

Chmykhova, N.M., O.A. Karamyan, and V.M. Kozhanov (1987) Morphological bases of interaction between motoneurons in spinal cord isolated from young rats using HRP techniques. Neurofiziologiya *20:*340–350.

Cox, D.R., and D.V. Hinkley (1974) Theoretical statistics. London: Chapman and Hall.

Cullheim, S., J.W. Fleshman, L.L. Glenn, and R.E. Burke (1987) Membrane area and dendritic structure in type identified triceps surae alpha motoneurons. J. Comp. Neurol. *255:*68–81.

De Ruiter, J.P. and H.B.M. Uylings (1987) Morphometric and dendritic analysis of fascia dentata granule cells in human aging and senile dementia. Brain Res. *402:*217–229.

De Schutter, E., and J.M. Bower (1994a) An active membrane model of the cerebellar Purkinje cell. I. Simulation of current clamps in slice. J. Neurophysiol. *71:*375–400.

De Schutter, E., and J.M. Bower (1994b) An active membrane model of the cerebellar Purkinje cell. II. Simulation of synaptic responses. J. Neurophysiol. *71:*401–419.

Dityatev, A.E., N.M. Chmykhova, L. Studer, O.A. Karamyan, V.M. Kozhanov, and H.P. Clamann (1995) Comparison of the topology and growth rules of motoneuronal dendrites. J. Comp. Neurol. *363:*505–516.

Hillman, D.E. (1979) Neuronal shape parameters and substructures as a basis of neuronal form. In F.O. Schmitt and F.G. Worden (eds): The Neurosciences, Fourth Study Program. Cambridge, MA: MIT Press, pp. 477–498.

Hillman, D.E. (1988) Parameters of dendritic shape and substructures: intrinsic and extrinsic determination? In R. Lasek and M. Black (eds): Intrinsic Determinants of Neuronal Form and Function. New York: Liss, pp. 83–113.

Kater, S.B., R.W. Davenport, and P.B. Guthrie (1994) Filopodia as detectors of environmental cues: Signal integration through changes in growth cone calcium levels. In J. van Pelt, M.A. Corner, H.B.M. Uylings, and F.H. Lopes da Silva (eds): The Self-Organizing Brain: From Growth Cones to Functional Networks, Progress in Brain Research, Vol. 102. Amsterdam: Elsevier, pp. 49–60.

Kliemann, W. (1987) A stochastic dynamical model for the characterization of the geometrical structure of dendritic processes. Bull. Math Biol. *49:*135–152.

Larkman, A.L. (1991) Dendritic morphology of pyramidal neurones of the visual cortex of the rat. I. Branching patterns. J. Comp. Neurol. *306:*307–310.

Letourneau, P.C., D.M. Snow, and T.M. Gomez (1994) Growth cone motility: substratum-bound molecules, cytoplasmic [Ca^{2+}] and Ca^{2+}-regulated proteins. In J. van Pelt, M.A. Corner, H.B.M. Uylings, and F.H. Lopes da Silva (eds): The Self-Organizing Brain: From Growth Cones to Functional Networks, Progress in Brain Research, Vol. 102. Amsterdam: Elsevier, pp. 35–48.

Martin, S.R., M.J. Schilstra, and P.M. Bayley (1993) Dynamic instability of microtubules: Monte Carlo simulation and application to different types of microtubule lattice. Biophys. J. *65:*578–596.

Núñez-Abades, P.A., F. He, G. Barrionuevo, and W.E. Cameron (1994) Morphology of developing rat genioglossal motoneurons studied in vitro: Changes in length, branching pattern, and spatial distribution of dendrites. J. Comp. Neurol. *339:*401–420.

Rall, W., R.E. Burke, W.R. Holmes, J.J.B. Jack, S.J. Redman, and I. Segev (1992) Matching dendritic neuron models to experimental data. Physiol. Rev. *72:* S159–S186.

Schierwagen, A.K. (1994) Exploring the computational capabilities of single neurons by continuous cable modeling. In J. van Pelt, M.A. Corner, H.B.M. Uylings, and F.H. Lopes da Silva (eds): Progress in Brain Research, Vol. 102, The Self-Organizing Brain: From Growth Cones to Functional Networks. Amsterdam: Elsevier, pp. 151–167.

Segev, I. (1992) Single neuron models: Oversimple, complex and reduced. Trends Neurosci. *15:*414–421.

Seress, L. and L. Mrzljak (1987) Basal dendrites of granule cells are normal features of the fetal and adult dentate gyrus of both monkey and human hippocampal formation. Brain Res. *405:*169–174.

Studer, L., C. Spenger, J. Luthman, and R.W. Seiler (1994) NGF increases neuritic complexity of cholinergic interneurons in organotypic cultures of neonatal rat striatum. J. Comp. Neurol. *340:*281–296.

Traub, R.D., and J.G.R. Jefferys (1994) Are there unifying principles underlying the generation of epileptic afterdischarges in vitro? In J. van Pelt, M.A. Corner, H.B.M. Uylings, and F.H. Lopes da Silva (eds): Progress in Brain Research, Vol. 102, The Self-Organizing Brain: From Growth Cones to Functional Networks. Amsterdam: Elsevier, pp. 383–394.

Uemura, E., A. Carriquiry, W. Kliemann, and J. Goodwin (1995) Mathematical modeling of dendritic growth in vitro. Brain Res. *671:*187–194.

Ulfhake, B., S. Cullheim, and P. Franson (1988) Postnatal development of cat hind limb motoneurons. I: Changes in length, branching structure, and spatial distribution of dendrites of cat triceps surae motoneurons. J. Comp. Neurol. *278:*69–87.

Ulfhake, B. and S. Cullheim (1988) Postnatal development of cat hindlimb motoneurons. II. In vivo morphology of dendritic growth cones and the maturation of dendritic morphology. J. Comp. Neurol. *278:*88–102.

Ulrich, D., R. Quadroni, and H.-R. Luscher (1994) Electrotonic structure of motoneurons in spinal cord slice cultures: A comparison of compartmental and equivalent cylinder models. J. Neurophysiol. *72:*861–871.

Uylings, H.B.M., J. van Pelt, R.W.H. Verwer, and P. McConnell (1989) Statistical analysis of neuronal populations. In J.J. Capowski (ed): Computer Techniques in Neuroanatomy. New York: Plenum, pp. 241–264.

Uylings, H.B.M., C.G. van Eden, J.G. Parnavelas, and A. Kalsbeek (1990) The prenatal and postnatal development of rat cerebral cortex. In B. Kolb and R.C. Tees (eds): The Cerebral Cortex of the Rat. Cambridge MA, MIT Press, pp. 35–76.

Uylings, H.B.M., J. van Pelt, J.G. Parnavelas, and A. Ruiz-Marcos (1994) Geometrical and topological characteristics in the dendritic development of cortical pyramidal and non-pyramidal neurons. In J. van Pelt, M.A. Corner, H.B.M. Uylings, and F.H. Lopes da Silva (eds): Progress in Brain Research, Vol. 102, The Self-Organizing Brain: From Growth Cones to Functional Networks. Amsterdam: Elsevier, pp. 109–123.

Van Pelt, J., and R.W.H. Verwer (1983) The exact probabilities of branching patterns under terminal and segmental growth hypotheses. Bull. Math. Biol. *45:*269–285.

Van Pelt, J., and R.W.H. Verwer (1986) Topological properties of binary trees grown with order-dependent branching probabilities. Bull. Math. Biol. *48:*197–211.

Van Pelt, J., H.B.M. Uylings, R.W.H. Verwer, R.J. Pentney, and M.J. Woldenberg (1992) Tree asymmetry: A sensitive and practical measure for binary topological trees. Bull. Math. Biol. *54:*759–784.

Van Pelt, J., A. van Ooyen, and M.A. Corner (1996) Growth cone dynamics and activity-dependent processes in neuronal network development. In R. Ranney Mize (ed): Neural Development and Plasticity, Progress in Brain Research, Vol. 108. Amsterdam: Elsevier, pp. 333–346.

Van Pelt, Jaap (1997) Effect of pruning on dendritic tree topology. J. Theor. Biol. *186:*17–32.

Van Veen, M.P., and J. van Pelt (1994) Dynamic mechanisms of neuronal outgrowth. In J. van Pelt, M.A. Corner, H.B.M. Uylings, and F.H. Lopes da Silva (eds): The Self-Organizing Brain: From Growth Cones to Functional Networks, Progress in Brain Research, Vol 102. Amsterdam: Elsevier, pp. 95–108.

Verwer, R.W.H., J. van Pelt, and A.J. Noest (1987) Parameter estimation in topological analysis of binary tree structures. Bull. Math. Biol. *49:*363–378.

Woldenberg, M.J., M.P. O'Neill, L.J. Quackenbush, and R.J. Pentney (1993) Models for growth, decline and regrowth of the dendrites of rat Purkinje cells induced from magnitude and link-length analysis. J. Theor. Biol. *162:*403–429.